CHALMERS
UNIVERSITY OF TECHNOLOGY

SISO RIS-Enabled Joint 3D Downlink Localization and Synchronization

Citation for the original published paper (version of record):
Keykhosravi, K., Keskin, F., Seco-Granados, G. et al (2021). SISO RIS-Enabled Joint 3D Downlink Localization and Synchronization. IEEE International Conference on Communications.
http://dx.doi.org/10.1109/ICC42927.2021.9500281

SISO RIS-Enabled Joint 3D Downlink Localization and Synchronization

Kamran Keykhosravi*, Musa Furkan Keskin*, Gonzalo Seco-Granados†, and Henk Wymeersch*
* Department of Electrical Engineering, Chalmers University of Technology, Sweden
† Department of Telecommunications and Systems Engineering, Universitat Autonòma de Barcelona, Spain
email: kamrank@chalmers.se

***Abstract*—We consider the problem of joint three-dimensional localization and synchronization for a single-input single-output (SISO) multi-carrier system in the presence of a reconfigurable intelligent surface (RIS), equipped with a uniform planar array. First, we derive the Cramér-Rao bounds (CRBs) on the estimation error of the channel parameters, namely, the angle-of-departure (AOD), composed of azimuth and elevation, from RIS to the user equipment (UE) and times-of-arrival (TOAs) for the path from the base station (BS) to UE and BS-RIS-UE reflection. In order to avoid high-dimensional search over the parameter space, we devise a low-complexity estimation algorithm that performs two 1D searches over the TOAs and one 2D search over the AODs. Simulation results demonstrate that the considered RIS-aided wireless system can provide submeter-level positioning and synchronization accuracy, materializing the positioning capability of Beyond 5G networks even with single-antenna BS and UE. Furthermore, the proposed estimator is shown to attain the CRB at a wide interval of distances between UE and RIS. Finally, we also investigate the scaling of the position error bound with the number of RIS elements.**

***Index Terms*—Reconfigurable intelligent surface, position error bound, Cramér-Rao bound, localization.**

I. Introduction

Provisioning of radio localization in cellular wireless communication standards was stirred by governmental requirements (Federal Communications Commission and European Commission) on locating the user equipment (UE) by the operators upon receiving an emergency call. Other applications include location-aware communication, geo-advertising, augmented reality, etc [1]. According to 3GPP standards, localization in 4G [2] can be obtained using time-difference-of-arrival measurements between a UE and multiple synchronized base stations (BSs). Since UE is not synchronized to the BSs, at least 4 BSs are needed to solve for the 3D UE position and the clock bias. Hence, cellular localization requires sufficient dense infrastructure and tight inter-BS synchronization. In the context of 5G, it has been shown that mmWave localization with a single BS is possible, provided that UE and BS are equipped with large arrays, and communicate under sufficiently rich multipath conditions [3]. By estimating angles-of-arrival (AOAs) and angles-of-departure (AODs) in addition to delays, localization and synchronization is possible, even when the multipath sources are a priori unknown [4]. Towards 6G, reconfigurable intelligent surfaces (RISs) deserve special attention among the technological enablers, since they can redirect strong signals from a BS towards a UE, thus boosting communication quality among other advantages [5]. In recent years, significant effort has been devoted to study manufacturing, channel models, control, performance gains, and topology design of RIS-aided communication system (see e.g., [6], [7]).

RISs have been considered as one of the main enabling technologies of beyond-5G localization [8], [9] and have been investigated in a number of studies in the localization literature, e.g., [10]–[15]. In [10], [11] localization in the near-field range of a RIS, functioning as a lens, is studied. Cramér Rao bounds (CRBs) have been derived in [12] for a 2D localization in presence of a large intelligent surface equipped with a uniform linear arry (ULA). In [13], authors have proposed a joint positioning and beam training algorithm for a wireless system comprising multiple RISs with ULAs. A single-input single-output 2D localization problem with synchronized signaling and multiple RISs (with ULA) has been investigated in [14] by deriving the CRB bounds. In [15], position error bounds (PEBs) have been derived for 3D uplink localization considering both synchronous and asynchronous cases. The authors pointed to the fact that the bounds can be attained by applying a grid search to maximize the log-likelihood function, however, no low-complexity estimation algorithm was presented.

In this paper, we study the 3D downlink localization and synchronization of a UE with a single antenna using the received line-of-sight (LOS) signal from a single-antenna BS and the reflected signal from a RIS with a uniform planar array (UPA). To the best of our knowledge, RIS-aided localization has never been studied in this elemental configuration. The contributions of this paper are:

- We show that both the 3D position and clock bias of the user can be estimated when both the BS and the UE have a single antenna, by the aid of a single RIS, provided that multiple distinct RIS phase profiles are used. As it is known, localization and synchronization would not be possible in the considered scenario without the RIS.
- We perform the Fisher information matrix (FIM) analysis and calculate the CRB bounds for the user position and channel parameters, showing that the localization is enabled by AOD estimation from the RIS.
- We provide a novel low-complexity localization and syn-

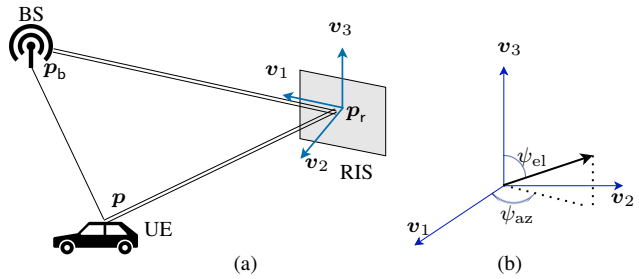

Fig. 1: (a): System setup, (b): Elevation and azimuth angles of a vector.

chronization method, which transforms the underlying 4-dimensional problem into two 1-dimensional and one two 2-dimensional problems. We also show that the proposed method attains the CRB bound.

The MATLAB implementation of the CRB calculations and the proposed estimation technique can be found in the repository [16].

Notation

Vectors and matrices are indicated by lowercase and uppercase bold letters resp. The element in the ith row and jth column of matrix $\boldsymbol{A}$ is specified by $[\boldsymbol{A}]_{i,j}$. Similarly, $[\boldsymbol{p}]_i$ indicates the ith element of vector $\boldsymbol{p}$. The subindex $i:j$ specifies all the elements between i and j. All vectors are columns, unless stated otherwise. By $\otimes$, we indicate the Kronecker product, and by $\mathrm{vec}(\cdot)$, the matrix vectorization operator. The complex conjugate, Hermitian, and transpose operators are represented by $(\cdot)^*$, $(\cdot)^\mathrm{H}$, and $(\cdot)^\top$, respectively.

II. System and Channel Model

A. System Setup

We consider a wireless system consisting of a single-antenna BS, a single-antenna UE, and a RIS. In Fig. 1a, the system setup is illustrated. The user receives the transmitted signal directly from BS (LOS path) and also from the RIS (reflected path). We assume that the position of the BS and the RIS ($\boldsymbol{p}_\mathrm{b}$ and $\boldsymbol{p}_\mathrm{r}$, respectively according to some general coordinate system) as well as the rotation matrix corresponding to the RIS coordinate system

$$\boldsymbol{R} \triangleq [\boldsymbol{v}_1, \boldsymbol{v}_2, \boldsymbol{v}_3]^\top \tag{1}$$

are known. On the other hand, the UE position ($\boldsymbol{p}$) is unknown and should be estimated. In addition, we consider an asynchronous scenario, where the user clock bias Δ_t should also be estimated. Fig. 1b presents the definition of azimuth and elevation of a general angle in the RIS coordinate system.

We assume that RIS is an M_r by M_c UPA with inter-element distance equal to d. In this case, the element in the ℓth row ($\ell \in \{0, \dots, M_\mathrm{r}-1\}$) and mth column ($m \in \{0, \dots, M_\mathrm{c}-1\}$) has the position $\boldsymbol{q}_{\ell,m} = [d\ell - d(M_\mathrm{r}-1)/2), 0, dm - d(M_\mathrm{c}-1)/2]$ in the RIS coordinate system. We assume that the RIS modulates the phase of the incident wave at time t according to the matrix $\boldsymbol{\Gamma}_t \in \mathbb{C}^{M_\mathrm{r} \times M_\mathrm{c}}$, where $|[\boldsymbol{\Gamma}_t]_{\ell,m}| = 1$ for all ℓ and m.

B. Signal Transmission

In this paper, we consider the transmission of T OFDM symbols with N subcarriers for one localization occasion. For simplicity, we assume that all the transmitted pilot symbols are equal to $\sqrt{E_\mathrm{s}}$. Then the received signal can be expressed as the $N \times T$ matrix

$$\boldsymbol{Y} = g_\mathrm{b}\sqrt{E_\mathrm{s}}\boldsymbol{d}(\tau_\mathrm{b})\boldsymbol{1}_T^\top + g_\mathrm{r}\sqrt{E_\mathrm{s}}\boldsymbol{d}(\tau_\mathrm{r})\boldsymbol{u}(\boldsymbol{\phi})^\top + \boldsymbol{N}, \tag{2}$$

where $\boldsymbol{Y} = [\boldsymbol{y}_0, \dots, \boldsymbol{y}_{T-1}]$, and $\boldsymbol{y}_t \in \mathbb{C}^N$ corresponds to the tth OFDM symbol. The noise matrix $\boldsymbol{N} \in \mathbb{C}^{N\times T}$ comprises zero-mean circularly-symmetric independent and identically distributed Gaussian elements with variance σ^2. The complex channel gain for the LOS path and the reflected path are indicated by g_b and g_r, respectively. The delays $\tau_\mathrm{b} = \|\boldsymbol{p} - \boldsymbol{p}_\mathrm{b}\|/c + \Delta_\mathrm{t}$ and $\tau_\mathrm{r} = \|\boldsymbol{p} - \boldsymbol{p}_\mathrm{r}\|/c + \|\boldsymbol{p}_\mathrm{b} - \boldsymbol{p}_\mathrm{r}\|/c + \Delta_\mathrm{t}$ account for the propagation distance LOS and reflected path delays, respectively, including the clock offset Δ_t. The effect of these delays on the signal is captured by the vectors $\boldsymbol{d}(\tau_\mathrm{b})$ and $\boldsymbol{d}(\tau_\mathrm{r})$, respectively, where we have defined

$$\boldsymbol{d}(\tau) = [1, e^{-j2\pi\tau\Delta f}, \dots, e^{-j2\pi\tau(N-1)\Delta f}]^\top \tag{3}$$

with Δf being the subcarrier spacing.

Furthermore, we have

$$\begin{aligned}[\boldsymbol{u}(\boldsymbol{\phi})]_t &= (\boldsymbol{a}(\boldsymbol{\theta}))^\top \mathrm{diag}(\boldsymbol{\gamma}_t)\boldsymbol{a}(\boldsymbol{\phi}) \\ &= \left(\boldsymbol{\gamma}_t^\top \odot (\boldsymbol{a}(\boldsymbol{\theta}))^\top\right)\boldsymbol{a}(\boldsymbol{\phi})\end{aligned} \tag{4}$$

where, $\boldsymbol{\theta} = [\theta_\mathrm{az}, \theta_\mathrm{el}]^\top$ represents the *known* AOA in azimuth and elevation from the BS to the RIS, and $\boldsymbol{\phi} = [\phi_\mathrm{az}, \phi_\mathrm{el}]^\top$ denotes the AOD from the RIS to the UE, with $\phi_\mathrm{az} = \mathrm{atan2}([\boldsymbol{s}]_2, [\boldsymbol{s}]_1)$ and $\phi_\mathrm{el} = \arccos([\boldsymbol{s}]_3/\|\boldsymbol{p} - \boldsymbol{p}_\mathrm{r}\|)$, where $\boldsymbol{s} = \boldsymbol{R}(\boldsymbol{p} - \boldsymbol{p}_\mathrm{r})$.

Moreover, we have $\boldsymbol{\gamma}_t = \mathrm{vec}(\boldsymbol{\Gamma}_t)$ and the response vector of the RIS for the angle $\boldsymbol{\psi} \in \{\boldsymbol{\phi}, \boldsymbol{\theta}\}$ is defined as $\boldsymbol{a}(\boldsymbol{\psi}) = \boldsymbol{a}_\mathrm{r}(\boldsymbol{\psi}) \otimes \boldsymbol{a}_\mathrm{c}(\boldsymbol{\psi})$ and

$$\boldsymbol{a}_\mathrm{r}(\boldsymbol{\psi}) = e^{j\beta_\mathrm{r}}[1, e^{-j[\boldsymbol{k}(\boldsymbol{\psi})]_1 d}, \dots, e^{-j[\boldsymbol{k}(\boldsymbol{\psi})]_1 (M_\mathrm{r}-1)d}]^\top \tag{5}$$

$$\boldsymbol{a}_\mathrm{c}(\boldsymbol{\psi}) = e^{j\beta_\mathrm{c}}[1, e^{-j[\boldsymbol{k}(\boldsymbol{\psi})]_3 d}, \dots, e^{-j[\boldsymbol{k}(\boldsymbol{\psi})]_3 (M_\mathrm{c}-1)d}]^\top \tag{6}$$

where $\beta_\mathrm{r} = [\boldsymbol{k}(\boldsymbol{\psi})]_1(M_\mathrm{r}-1)d/2$ and $\beta_\mathrm{c} = [\boldsymbol{k}(\boldsymbol{\psi})]_3(M_\mathrm{c}-1)d/2$. Here,

$$\boldsymbol{k}(\boldsymbol{\psi}) = -\frac{2\pi}{\lambda}[\sin\psi_\mathrm{el}\cos\psi_\mathrm{az}, \sin\psi_\mathrm{el}\sin\psi_\mathrm{az}, \cos\psi_\mathrm{el}]^\top \tag{7}$$

is the wavenumber vector and λ is the carrier wavelength. Here, we assume that the wavelength remains relatively constant within the transmission bandwidth.

C. Goal

Our goal is to estimate the UE location $\boldsymbol{p}$ and its clock bias Δ_t from the observation $\boldsymbol{Y}$, given the RIS phase profiles, the transmitted signals, as well as location and orientation of the BS and RIS.

III. Fisher Information Analysis

A. FIM Derivation

In this section, we calculate the PEB, which is a lower bound on the root mean square error (RMSE) of any unbiased estimator of the position upon observing $\boldsymbol{Y}$. The PEB can be calculated as

$$\text{PEB} = \sqrt{\text{tr}\left(\left[\boldsymbol{F}_{\text{po}}^{-1}\right]_{1:3,1:3}\right)} \tag{8}$$

where $\boldsymbol{F}_{\text{po}}$ is the FIM of positional parameters

$$\boldsymbol{\zeta}_{\text{po}} = [\boldsymbol{p}^\top, \Delta_{\text{t}}, g_{\text{b,i}}, g_{\text{b,r}}, g_{\text{r,i}}, g_{\text{r,r}}]^\top. \tag{9}$$

Here, the subindices r and i indicate the real and imaginary parts, respectively, of the path gains g_{b} and g_{r}. We can calculate $\boldsymbol{F}_{\text{po}}$ based on the Fisher information of the channel parameters $\boldsymbol{F}_{\text{ch}}$ as $\boldsymbol{F}_{\text{po}} = \boldsymbol{J}^\top \boldsymbol{F}_{\text{ch}} \boldsymbol{J}$. The Jacobian matrix $\boldsymbol{J} \in \mathbb{R}^{8\times 8}$ is defined as

$$\boldsymbol{J}_{\ell,s} = \frac{\partial[\boldsymbol{\zeta}_{\text{ch}}]_\ell}{\partial[\boldsymbol{\zeta}_{\text{po}}]_s} \tag{10}$$

where $\boldsymbol{\zeta}_{\text{ch}} = [\tau_{\text{b}}, \tau_{\text{r}}, \phi_{\text{az}}, \phi_{\text{el}}, g_{\text{b,i}}, g_{\text{b,r}}, g_{\text{r,i}}, g_{\text{r,r}}]^\top$ is the set of channel parameters. $\boldsymbol{F}_{\text{ch}}$ can be written as

$$\boldsymbol{F}_{\text{ch}} = \frac{2}{\sigma^2} \sum_{t=0}^{T-1} \sum_{n=0}^{N-1} \text{Re}\left\{ \frac{\partial[\boldsymbol{E}]_{n,t}}{\partial \boldsymbol{\zeta}_{\text{ch}}} \left(\frac{\partial[\boldsymbol{E}]_{n,t}}{\partial \boldsymbol{\zeta}_{\text{ch}}} \right)^{\text{H}} \right\} \tag{11}$$

where $\boldsymbol{E} \in \mathbb{C}^{N\times T}$ is the noiseless part of the received signal in (2). The matrices $\boldsymbol{F}_{\text{ch}}$ and $\boldsymbol{J}$ needed to calculate the PEB are derived in Appendix A and Appendix B, respectively.

The CRB bound can be calculated also for Δ_{t} and the channel parameters. As an example, the CRB bound for Δ_{t} can be represented as

$$\sqrt{\mathbb{E}[(\Delta_{\text{t}} - \hat{\Delta}_t)^2]} \geq \sqrt{[\boldsymbol{F}_{\text{po}}^{-1}]_{4,4}} \tag{12}$$

where $\tilde{\Delta}_t$ indicates the estimate of the true time bias Δ_{t} and $\mathbb{E}$ represents the expectation over noise.

B. FIM Interpretation

We observe that the FIM involves a sum of rank-2 matrices over T transmissions and N subcarriers. As the dimension of $\boldsymbol{F}_{\text{ch}}$ is 8×8, it immediately follows that $TN \geq 4$ is a necessary condition for the problem to be identifiable. On the other hand, setting $N > 1$ is required to be able to estimate any of the delays, while $T > 1$ is needed to estimate the AODs. From [17], it is known that in order for the AOD to be identifiable, we need that the RIS phase profile vectors $\boldsymbol{\gamma}_t$'s at different transmission instances are not all parallel.

From a geometric point of view, it can be shown that the four channel geometric parameters (i.e., the two delays and the two AODs for azimuth and elevation) determine the four positional parameters (the 3D localization as the intersection between the AOD line and one-half of a two-sheet hyperboloid, and the clock bias). There is a one-to-one mapping between the channel geometric and the positional parameters, which is equivalent to the fact that the Jacobian $\boldsymbol{J}$ is an invertible matrix.

IV. Low-complexity Estimation

In this section, we develop an estimator to determine the channel parameters in $\boldsymbol{\zeta}_{\text{ch}}$ based on the received signal $\boldsymbol{Y}$, and then give an estimation of the UE position and clock bias based on the channel parameters. We first estimate τ_{b} and τ_{r} using IFFT of the received signal and then $\boldsymbol{\phi}$ based on the 2D-IFFT of the RIS phase profile matrices. At the end of each step, a *quasi-Newton* algorithm is used to refine the estimation.

A. Estimation of τ_{b}

We estimate τ_{b} based on the sum of the columns of $\boldsymbol{Y}$, $\boldsymbol{y}_{\text{c}} = \sum_t \boldsymbol{y}_t$, with

$$\begin{aligned} \boldsymbol{y}_{\text{c}} &= g_{\text{b}}\sqrt{E_{\text{s}}}\boldsymbol{d}(\tau_{\text{b}})\boldsymbol{1}_T^\top \boldsymbol{1}_T + g_{\text{r}}\sqrt{E_{\text{s}}}\boldsymbol{d}(\tau_{\text{r}})\boldsymbol{u}(\boldsymbol{\phi})^\top \boldsymbol{1}_T + \boldsymbol{N}\boldsymbol{1}_T, \\ &\approx T g_{\text{b}}\sqrt{E_{\text{s}}}\boldsymbol{d}(\tau_{\text{b}}) + \sum_t \boldsymbol{n}_t \end{aligned} \tag{13}$$

where $\boldsymbol{n}_t$ represents the tth column of matrix $\boldsymbol{N}$. This operation adds coherently the T transmissions for the LOS path, whereas this does not happen for the signal reflected by the RIS. We assume that T times the received power from the BS is much greater than the received power from RIS, which is a relevant assumption, especially when both BS and UE are in the far-field of RIS.

Next, we calculate the IFFT of the vector $\boldsymbol{y}_{\text{c}}$, that is $\bar{\boldsymbol{y}}_{\text{c}} = \boldsymbol{F}\boldsymbol{y}_{\text{c}}$, where $\boldsymbol{F} \in \mathbb{C}^{N_{\text{F}}\times N}$ is the IFFT matrix with elements

$$\boldsymbol{F}_{\ell,m} = \frac{1}{N_F} e^{2j\pi\ell m/N_F} \tag{14}$$

where N_{F} determines the length of the IFFT vector. If

$$\tau_{\text{b}} = \ell/(N_F \Delta f) \tag{15}$$

for some integer ℓ, the absolute value of the elements of $\bar{\boldsymbol{y}}_{\text{c}}$ will likely have a maximum around ℓ. However, with probability one, this assumption does not hold. Therefore, to obtain a more accurate estimation of τ_{b} we induce some artificial delay δ by calculating $\boldsymbol{y}_{\text{c}}(\delta) \triangleq \boldsymbol{y}_{\text{c}} \odot \boldsymbol{d}(\delta)$. First, we set $\delta = 0$ and calculate $\tilde{k} = \arg\max_k |\boldsymbol{e}_k^\top \boldsymbol{F}\boldsymbol{y}_{\text{c}}(0)|$, where $\boldsymbol{e}_k$ is vector comprising all zeros, except with a 1 in the kth entry. Next, we refine our estimation by calculating

$$\tilde{\delta} = \arg \max_{\delta\in[0,1/(N_F\Delta f)]} \left|\boldsymbol{e}_{\tilde{k}}^\top \boldsymbol{F}\boldsymbol{y}_{\text{c}}(\delta)\right|. \tag{16}$$

Then τ_{b} can be estimated as

$$\tilde{\tau}_{\text{b}} = \tilde{k}/(N_F\Delta f) - \tilde{\delta}. \tag{17}$$

Based on our numerical observation, the optimization over δ can be performed by a quasi-Newton method using 0 as starting point. We note that the purpose of auxiliary parameter δ is to add an artificial delay to the signal such that $\tau_{\text{b}} + \delta$ satisfies the condition (15), therefore, it is sufficient to constrain the range of δ in (16) to $[0, 1/(N_F\Delta f)]$.

B. Estimation of τ_{r}

To estimate τ_{r}, we first remove the BS contribution from the received signal $\boldsymbol{Y}$ by computing

$$\boldsymbol{Y}_{\mathsf{r}} = \boldsymbol{Y} - \tilde{g}_{\mathsf{b}}\boldsymbol{d}(\tilde{\tau}_{\mathsf{b}})\mathbf{1}_T^\top \tag{18}$$

$$\approx g_{\mathsf{r}}\sqrt{E_{\mathrm{s}}}\boldsymbol{d}(\tau_{\mathsf{r}})\boldsymbol{u}(\boldsymbol{\phi})^\top + \boldsymbol{N}, \tag{19}$$

where

$$\tilde{g}_{\mathsf{b}} = \frac{1}{TN}\sum_{n=0}^{N-1}[\boldsymbol{y}_{\mathrm{c}} \odot \boldsymbol{d}(-\tilde{\tau}_{\mathsf{b}})]_n \tag{20}$$

Then, similarly as in Section IV-A, we first perform the optimization

$$\tilde{k} = \arg\max_k \left\|\boldsymbol{e}_k^\top(\boldsymbol{F}\boldsymbol{Y}_{\mathsf{r}})\right\| \tag{21}$$

where $\boldsymbol{e}_k^\top(\boldsymbol{F}\boldsymbol{Y}_{\mathsf{r}})$ extracts the k-th row from the IFFT of $\boldsymbol{Y}_{\mathsf{r}}$. To refine the estimate, we calculate

$$\tilde{\delta} = \arg\max_{\delta\in[0,1/(N_F\Delta f)]} \left\|\boldsymbol{e}_k^\top\boldsymbol{F}\left(\boldsymbol{Y}_{\mathsf{r}} \odot \boldsymbol{d}(\delta)\mathbf{1}_T^\top\right)\right\|. \tag{22}$$

Finally similarly as in (17), we have $\tilde{\tau}_{\mathsf{r}} = \tilde{k}/(N_F\Delta f) - \tilde{\delta}$.

C. Estimation of $\boldsymbol{\phi}$

To estimate $\boldsymbol{\phi}$, we first remove the delay effects of the reflected path from the signal $\boldsymbol{Y}_{\mathsf{r}}$ by calculating

$$\boldsymbol{Y}_{\boldsymbol{\phi}} = \boldsymbol{Y}_{\mathsf{r}} \odot \boldsymbol{d}(-\tilde{\tau}_{\mathsf{r}})\mathbf{1}_T^\top. \tag{23}$$

Next, we sum over all the rows of $\boldsymbol{Y}_{\boldsymbol{\phi}}$ to obtain $\boldsymbol{y}_{\boldsymbol{\phi}} \in \mathbb{C}^{T\times 1}$. One can see from (2) that

$$\boldsymbol{y}_{\boldsymbol{\phi}} = \boldsymbol{Y}_{\boldsymbol{\phi}}^\top\mathbf{1}_N \tag{24}$$

$$\approx N g_{\mathsf{r}}\sqrt{E_{\mathrm{s}}}\boldsymbol{u}(\boldsymbol{\phi}) + \boldsymbol{N}^\top\mathbf{1}_N. \tag{25}$$

To estimate $\boldsymbol{\phi}$ based on $\boldsymbol{y}_{\boldsymbol{\phi}}$, we use the properties of the Kronecker product and vec operator [18, Eq. (520)], and based on (4), we obtain

$$[\boldsymbol{u}(\boldsymbol{\phi})]_t = e^{-j(\beta_{\mathrm{r}}+\beta_{\mathrm{c}})}\boldsymbol{a}_{\mathrm{c}}(\boldsymbol{\phi})^\top\left(\boldsymbol{\Gamma}_t \odot \boldsymbol{A}(\boldsymbol{\theta})\right)\boldsymbol{a}_{\mathrm{r}}(\boldsymbol{\phi}) \tag{26}$$

where $\boldsymbol{A}(\boldsymbol{\theta}) = \boldsymbol{a}_{\mathrm{c}}(\boldsymbol{\theta})\boldsymbol{a}_{\mathrm{r}}(\boldsymbol{\theta})^\top$. Motivated by (26), we search for $\boldsymbol{\phi}$ through taking 2D IFFT of the known matrices $\boldsymbol{\Gamma}_t \odot \boldsymbol{A}(\boldsymbol{\theta})$ as

$$\bar{\boldsymbol{\Gamma}}_t = \boldsymbol{F}_{\mathrm{r}}\left(\boldsymbol{\Gamma}_t \odot \boldsymbol{A}(\boldsymbol{\theta})\right)\boldsymbol{F}_{\mathrm{c}}^\top. \tag{27}$$

The matrices $\boldsymbol{F}_{\mathrm{r}} \in \mathbb{C}^{N_{\mathrm{F_r}}\times M_{\mathrm{r}}}$ and $\boldsymbol{F}_{\mathrm{c}} \in \mathbb{C}^{N_{\mathrm{F_c}}\times M_{\mathrm{c}}}$ are defined similarly as in (14), where $N_{\mathrm{F_r}}$ and $N_{\mathrm{F_c}}$ determine the dimensions of the 2D IFFT transforms. We note that matrices $\bar{\boldsymbol{\Gamma}}_t$ do not depend on the received signal and can be calculated offline.

Now, lets assume that for some integers $0 \le \ell \le N_{\mathrm{F_r}} - 1$ and $0 \le m \le N_{\mathrm{F_c}} - 1$, we have

$$[\boldsymbol{k}(\boldsymbol{\phi})]_1 d \equiv -2\pi\ell/N_{\mathrm{F_r}} \mod 2\pi \tag{28}$$

$$[\boldsymbol{k}(\boldsymbol{\phi})]_3 d \equiv -2\pi m/N_{\mathrm{F_c}} \mod 2\pi. \tag{29}$$

Then, by comparing (26) and (27), one can see that for some complex scalar ξ we have

$$\boldsymbol{\eta}_{\ell,m} \triangleq \left[[\bar{\boldsymbol{\Gamma}}_0]_{\ell,m}, \ldots, [\bar{\boldsymbol{\Gamma}}_{T-1}]_{\ell,m}\right]^\top = \xi\boldsymbol{u}(\boldsymbol{\phi}). \tag{30}$$

TABLE I: Parameters used in the simulation.

Parameter	Symbol	Value
RIS dimensions	$M_{\mathrm{r}} \times M_{\mathrm{c}}$	64×64
Wavelength	λ	1 cm
RIS element distance	d	0.5 cm
Light speed	c	3×10^8 m/s
Number of subcarriers	N	3 000
Subcarrier bandwidth	Δf	120 kHz
Number of transmissions	T	256
Transmission Power	NE_{s}	20 dBm
Noise PSD	N_0	-174 dBm/Hz
UE's Noise figure	n_f	8 dB
Noise variance	$\sigma^2 = n_f N_0 \Delta f$	-115.2 dBm
BS position	$\boldsymbol{p}_{\mathsf{b}}$	$[5, 5, 0]$
IFFT dimensions	N_{F}	4096
2-D IFFT dimensions	$N_{\mathrm{F_r}} = N_{\mathrm{F_c}}$	256

Motivated by (30) and (25), we find $\tilde{\ell}$ and $\tilde{m}$ such that $[\tilde{\ell}, \tilde{m}] = \arg\min_{\ell,m} w_{\ell,m}$, where

$$w_{\ell,m} \triangleq \left\|\boldsymbol{y}_{\boldsymbol{\phi}} - h\big(\boldsymbol{\eta}_{\ell,m}\big)\,\boldsymbol{\eta}_{\ell,m}\right\|^2 \tag{31}$$

where function $h(\boldsymbol{\eta}_{\ell,m})$ returns a scalar that minimizes the RHS of (31) for a given vector $\boldsymbol{\eta}_{\ell,m}$ and is defined as

$$h(\boldsymbol{v}) \triangleq \frac{\boldsymbol{v}^{\mathrm{H}}\boldsymbol{y}_{\boldsymbol{\phi}}}{\boldsymbol{v}^{\mathrm{H}}\boldsymbol{v}}. \tag{32}$$

Next, we use a quadratic interpolation to obtain continuous (and more accurate) values for $\tilde{\ell}, \tilde{m}$, i.e., we calculate

$$\ell_{\mathrm{q}} = \tilde{\ell} + \frac{w_{\ell-1,m} - w_{\ell+1,m}}{2(w_{\ell-1,m} + w_{\ell+1,m} - 2w_{\ell,m})}. \tag{33}$$

Also, we calculate m_{q} similarly to (33). Next, based on ℓ_{q} and m_{q}, we estimate $[\boldsymbol{k}(\boldsymbol{\phi})]_1$ and $[\boldsymbol{k}(\boldsymbol{\phi})]_3$ using (28)–(29) and calculate an estimation of $\boldsymbol{\phi}$ using the following relations

$$[\boldsymbol{k}(\boldsymbol{\phi})]_2 = -\sqrt{4\pi^2/\lambda^2 - ([\boldsymbol{k}(\boldsymbol{\phi})]_1)^2 - ([\boldsymbol{k}(\boldsymbol{\phi})]_3)^2} \tag{34}$$

$$\phi_{\mathsf{az}} = \operatorname{atan2}\left(-[\boldsymbol{k}(\boldsymbol{\phi})]_2, -[\boldsymbol{k}(\boldsymbol{\phi})]_1\right) \tag{35}$$

$$\phi_{\mathsf{el}} = \operatorname{acos}\left(-\lambda[\boldsymbol{k}(\boldsymbol{\phi})]_3/2\pi\right). \tag{36}$$

Finally, we refine our estimation by performing the minimization

$$\tilde{\boldsymbol{\phi}} = \arg\min_{\boldsymbol{\psi}} \left\|\boldsymbol{y}_{\boldsymbol{\phi}} - h(\boldsymbol{u}(\boldsymbol{\psi}))\,\boldsymbol{u}(\boldsymbol{\psi})\right\| \tag{37}$$

where $\boldsymbol{u}(\boldsymbol{\psi})$ is defined in (4). We solve (37) by applying the quasi-Newton algorithm, using (35) and (36) as the initial point.

D. Estimation of UE position and clock bias

The UE position is calculated as $\tilde{\boldsymbol{p}} = \boldsymbol{p}_{\mathsf{r}} + \tilde{\kappa}\boldsymbol{R}^\top\boldsymbol{k}(\tilde{\boldsymbol{\phi}})$, where $\boldsymbol{k}(\tilde{\boldsymbol{\phi}})$ is defined in (7) and

$$\tilde{\kappa} = \arg\min_{\kappa}\Big(\|\kappa\boldsymbol{R}^\top\boldsymbol{k}(\tilde{\boldsymbol{\phi}})\| + \|\boldsymbol{p}_{\mathsf{b}} - \boldsymbol{p}_{\mathsf{r}}\| - \left\|\boldsymbol{p}_{\mathsf{b}} - \boldsymbol{p}_{\mathsf{r}} - \kappa\boldsymbol{R}^\top\boldsymbol{k}(\tilde{\boldsymbol{\phi}})\right\| - (\tilde{\tau}_{\mathsf{r}} - \tilde{\tau}_{\mathsf{b}})c\Big)^2 \tag{38}$$

where c is the speed of the light. The value of $\tilde{\kappa}$ can be found numerically via a gradient-descent algorithm. Then we estimate the clock bias as

$$\tilde{\Delta}_t = \tilde{\tau}_{\mathsf{b}} - \|\tilde{\boldsymbol{p}} - \boldsymbol{p}_{\mathsf{b}}\|/c. \tag{39}$$

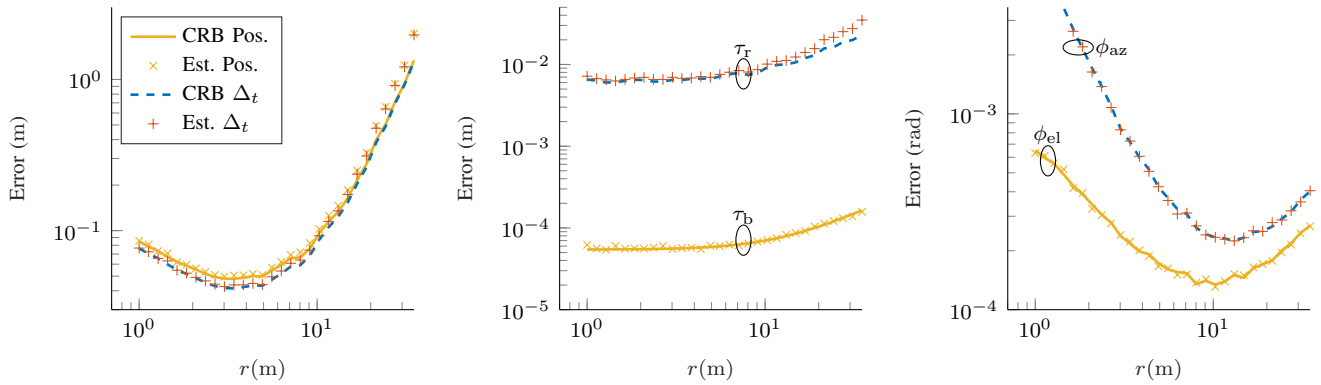

Fig. 2: Estimation error (markers) and the CRB bounds (lines) for user position, time bias Δ_t, AOD elevation ϕ_{el}, AOD azimuth ϕ_{az}, LOS delay τ_b, and reflected path delay τ_r, along the path $[-r/\sqrt{2}, r/\sqrt{2}, -10]$, where $r \in [1\ 35]$.

Complexity: Finally, we note that the estimation of the channel parameters can also be done by searching over the parameters $[\tau_b, \tau_r, \phi_{az}, \phi_{el}]$ to maximize the likelihood function (or minimize the squared error function). However, this four-dimensional search would be much more complex than our method which has two one-dimensional and one two-dimensional search.

V. Simulation Results

In this section, we evaluate the CRB presented in Sec. III and compare them to the RMSE of the estimator proposed in Sec. IV. We study also the effect of the number of RIS elements on PEB. To evaluate the estimator performance, we average over 1 000 noise realizations. For each noise realization, Δ_t is set to a random number uniformly drawn from the interval $[0, 1/\Delta f)$. It is assumed that the RIS and the BS are at the same height, while UE is placed 10 meters below them. The absolute coordinate system is set to be aligned with the RIS coordinates, i.e., $\boldsymbol{R}$ is an identity matrix and $\boldsymbol{p}_r = [0, 0, 0]$. All the phase shifts of the RIS elements are drawn from a uniform distribution over $[0, 2\pi)$, independently. The amplitude of the channel gains g_b and g_r are calculated based on Friis' formula (using unit directivity for BS, UE, and RIS elements) and their phase are set randomly between $[0, 2\pi)$. The rest of the parameters are presented in Table I.

Fig. 2 illustrates the CRB and the estimation errors for the UE position, clock bias, and channel parameters along the direction $[-r/\sqrt{2}, r/\sqrt{2}, -10]$. As can be seen, positioning with submeter accuracy is possible for $r < 30$. One can see that the proposed estimator is operating in close vicinity of the theoretical bounds. With low values of r, the UE is positioned almost beneath RIS and a relatively poor angle estimation is obtained. With $r > 10\text{m}$ the estimation performance deteriorates with r for all the parameters as the signal-to-noise ratio (SNR) decreases. As can be seen, the estimation error of Δ_t is close to the PEB bound. This can be explained based on (39) and the fact that the error in τ_b is much less than the position error.

In Fig. 3, we illustrate the effect of the RIS size on the PEB bound at five different locations. A RIS with the same number of rows and columns is considered. One can see that for all the considered points, the decrease in the PEB is proportional to the square-root of the number of the RIS elements. This is due to the SNR increase of the reflected path, which is proportional to the number of RIS elements, and the fact that there is no significant beamforming gain because the phase shifts are random.

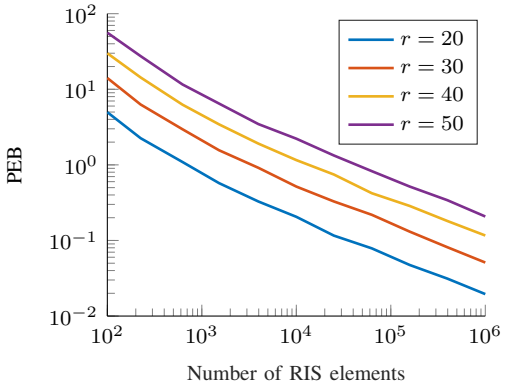

Fig. 3: PEB for different numbers of RIS elements. Four different points are considered: $[-r/\sqrt{2}, r/\sqrt{2}, -10]$ with $r \in \{20, 30, 40, 50\}$.

VI. Conclusion

We have investigated localization and synchronization in a wireless system with a single-antenna UE, a single-antenna BS, and a RIS. We have calculated the Cramér-Rao bounds and derived a low-complexity estimator to determine the AOD from the RIS, and the delays of the direct and reflected signals. Then based on these parameters, we have estimated the user position and its clock bias. By comparing the estimator's error to the CRBs we have shown that our estimator is efficient and that 3D localization and synchronization is possible for the considered system. Our results point to the potential of RIS in enabling radio localization for simple wireless networks. A future research direction is to investigate the multi-user scenario and to study the effects of employing multi-antenna BS, different RIS phase profiles, and different pilots' energy levels on the localization performance in the considered setup.

ACKNOWLEDGMENTS

This work was supported, in part, by the Swedish Research Council under grant 2018-03701, the Marie Skłodowska-Curie Individual Fellowships (H2020-MSCA-IF-2019) Grant 888913 (OTFS-RADCOM), the Spanish Ministry of Science, Innovation and Universities under Projects TEC2017-89925-R and PRX18/00638 and by the ICREA Academia Programme.

APPENDIX A
CALCULATING $\boldsymbol{F}_{\rm ch}$

In this appendix, we derive $\partial[\boldsymbol{E}]_{n,t}/\partial[\boldsymbol{\zeta}_{\rm ch}]_r$, then elements of $\boldsymbol{F}_{\rm ch}$ can be calculated from (11). We have

$$\frac{\partial[\boldsymbol{E}]_{n,t}}{\partial\tau_{\mathsf{b}}} = -j2\pi n\Delta f g_{\mathsf{b}}\sqrt{E_{\rm s}}e^{-j2\pi n\tau_{\mathsf{b}}\Delta f} \tag{40}$$

$$\frac{\partial[\boldsymbol{E}]_{n,t}}{\partial\tau_{\mathsf{r}}} = -j2\pi n\Delta f g_{\mathsf{r}}\sqrt{E_{\rm s}}e^{-j2\pi n\tau_{\mathsf{r}}\Delta f}[\boldsymbol{u}(\boldsymbol{\phi})]_t \tag{41}$$

$$\frac{\partial[\boldsymbol{E}]_{n,t}}{\partial\phi_{\rm az}} = g_{\mathsf{r}}\sqrt{E_{\rm s}}e^{-j2\pi n\tau_{\mathsf{r}}\Delta f}\left(\frac{\partial\boldsymbol{a}(\boldsymbol{\phi})}{\partial\phi_{\rm az}}\right)^{\top}\boldsymbol{z}_t \tag{42}$$

$$\frac{\partial[\boldsymbol{E}]_{n,t}}{\partial\phi_{\rm el}} = g_{\mathsf{r}}\sqrt{E_{\rm s}}e^{-j2\pi n\tau_{\mathsf{r}}\Delta f}\left(\frac{\partial\boldsymbol{a}(\boldsymbol{\phi})}{\partial\phi_{\rm el}}\right)^{\top}\boldsymbol{z}_t \tag{43}$$

where $\boldsymbol{z}_t = \boldsymbol{\gamma}_t \odot \boldsymbol{a}(\boldsymbol{\theta})$ and

$$\frac{\partial\boldsymbol{a}(\boldsymbol{\phi})}{\partial\phi_{\rm az}} = \boldsymbol{a}(\boldsymbol{\phi}) \odot \left(-j(\frac{\partial\boldsymbol{k}(\boldsymbol{\phi})}{\partial\phi_{\rm az}})^{\top}\boldsymbol{Q}\right) \tag{44}$$

$$\frac{\partial\boldsymbol{a}(\boldsymbol{\phi})}{\partial\phi_{\rm el}} = \boldsymbol{a}(\boldsymbol{\phi}) \odot \left(-j(\frac{\partial\boldsymbol{k}(\boldsymbol{\phi})}{\partial\phi_{\rm el}})^{\top}\boldsymbol{Q}\right) \tag{45}$$

$$\frac{\partial\boldsymbol{k}(\boldsymbol{\phi})}{\partial\phi_{\rm az}} = -\frac{2\pi}{\lambda_n}[-\sin\phi_{\rm el}\sin\phi_{\rm az}, \sin\phi_{\rm el}\cos\phi_{\rm az}, 0]^{\top} \tag{46}$$

$$\frac{\partial\boldsymbol{k}(\boldsymbol{\phi})}{\partial\phi_{\rm el}} = -\frac{2\pi}{\lambda_n}[\cos\phi_{\rm el}\cos\phi_{\rm az}, \cos\phi_{\rm el}\sin\phi_{\rm az}, -\sin\phi_{\rm el}]^{\top} \tag{47}$$

$$\boldsymbol{Q} = [\boldsymbol{q}_{0,0}, \boldsymbol{q}_{1,0}, \ldots, \boldsymbol{q}_{M_{\rm r}-1,M_{\rm c}-1}]. \tag{48}$$

Finally, for gains, we have

$$[\frac{\partial[\boldsymbol{E}]_{n,t}}{\partial g_{\mathsf{b,r}}}, \frac{\partial[\boldsymbol{E}]_{n,t}}{\partial g_{\mathsf{b,i}}}] = \sqrt{E_{\rm s}}e^{-j2\pi n\tau_{\mathsf{b}}\Delta f}[1, j] \tag{49}$$

$$[\frac{\partial[\boldsymbol{E}]_{n,t}}{\partial g_{\mathsf{r,r}}}, \frac{\partial[\boldsymbol{E}]_{n,t}}{\partial g_{\mathsf{r,i}}}] = \sqrt{E_{\rm s}}e^{-j2\pi n\tau_{\mathsf{r}}\Delta f}[\boldsymbol{u}(\boldsymbol{\phi})]_t[1, j]. \tag{50}$$

APPENDIX B
CALCULATING $\boldsymbol{J}$

According to (10), to determine the elements of $\boldsymbol{J}$, one should calculate the derivatives $\partial[\boldsymbol{\zeta}_{\rm ch}]_r/\partial[\boldsymbol{\zeta}_{\rm po}]_s$. To do so, we first write each element of $\boldsymbol{\zeta}_{\rm ch}$ as a function of $\boldsymbol{\zeta}_{\rm po}$, as described in Section II-B and then calculate the derivatives.

For any function f, we use the notation $\partial f/\partial\boldsymbol{p} \in \mathbb{R}^3$ to denote the gradient of f with respect to variable $\boldsymbol{p}$.

$$\frac{\partial\tau_{\mathsf{b}}}{\partial\boldsymbol{p}} = \frac{1}{c}\frac{\boldsymbol{p}-\boldsymbol{p}_{\mathsf{b}}}{\|\boldsymbol{p}-\boldsymbol{p}_{\mathsf{b}}\|} \tag{51}$$

$$\frac{\partial\tau_{\mathsf{r}}}{\partial\boldsymbol{p}} = \frac{1}{c}\frac{\boldsymbol{p}-\boldsymbol{p}_{\mathsf{r}}}{\|\boldsymbol{p}-\boldsymbol{p}_{\mathsf{r}}\|} \tag{52}$$

$$[\frac{\partial\tau_{\mathsf{b}}}{\partial\Delta_{\mathsf{t}}}, \frac{\partial\tau_{\mathsf{r}}}{\partial\Delta_{\mathsf{t}}}] = [1, 1]. \tag{53}$$

For the AOD from RIS to UE, $\boldsymbol{\phi}$, we have

$$\frac{\partial\phi_{\rm az}}{\partial\boldsymbol{p}} = \frac{1}{([\boldsymbol{s}]_1)^2+([\boldsymbol{s}]_2)^2}[-[\boldsymbol{s}]_2\boldsymbol{R}_{1,1:3}+[\boldsymbol{s}]_1\boldsymbol{R}_{2,1:3}] \tag{54}$$

$$\frac{\partial\phi_{\rm el}}{\partial\boldsymbol{p}} = \frac{-\|\boldsymbol{s}\|^2[\boldsymbol{R}]_{3,1:3}+(\boldsymbol{p}-\boldsymbol{p}_{\mathsf{r}})[\boldsymbol{s}]_3}{\|\boldsymbol{s}\|^2\sqrt{([\boldsymbol{s}]_1)^2+([\boldsymbol{s}]_2)^2}}. \tag{55}$$

Furthermore, we have

$$[\frac{\partial g_{\mathsf{b,r}}}{\partial g_{\mathsf{b,r}}}, \frac{\partial g_{\mathsf{b,i}}}{\partial g_{\mathsf{b,i}}}, \frac{\partial g_{\mathsf{r,r}}}{\partial g_{\mathsf{r,r}}}, \frac{\partial g_{\mathsf{r,i}}}{\partial g_{\mathsf{r,i}}}] = [1, 1, 1, 1]. \tag{56}$$

The rest of the derivatives are zero.

REFERENCES

[1] J. A. del Peral-Rosado, R. Raulefs, J. A. López-Salcedo, and G. Seco-Granados, "Survey of cellular mobile radio localization methods: From 1G to 5G," *IEEE Commun. Surveys Tutorials*, vol. 20, no. 2, pp. 1124–1148, 2018.

[2] "Feasibility of positioning enhancements for E-UTRA, release 13, V13.0.0," 3GPP TR 36.855, Jan. 2015.

[3] A. Shahmansoori, G. E. Garcia, G. Destino, G. Seco-Granados, and H. Wymeersch, "Position and orientation estimation through millimeter-wave MIMO in 5G systems," *IEEE Trans. Wireless Commun.*, vol. 17, no. 3, pp. 1822–1835, Mar. 2018.

[4] H. Wymeersch, N. Garcia, H. Kim, G. Seco-Granados, S. Kim, F. Wen, and M. Fröhle, "5G mm wave downlink vehicular positioning," in *IEEE Global Commun. Conf. (GLOBECOM).*, Abu Dhabi, UAE, Dec. 2018, pp. 206–212.

[5] E. Basar, M. Di Renzo, J. De Rosny, M. Debbah, M. Alouini, and R. Zhang, "Wireless communications through reconfigurable intelligent surfaces," *IEEE Access*, vol. 7, pp. 116 753–116 773, Sep. 2019.

[6] D. Dardari, "Communicating with large intelligent surfaces: Fundamental limits and models," *IEEE J. Select. Areas Commun.*, vol. 38, no. 11, pp. 2526–2537, Jul. 2020.

[7] N. S. Perović, M. D. Renzo, and M. F. Flanagan, "Channel capacity optimization using reconfigurable intelligent surfaces in indoor mmwave environments," in *IEEE Int. Conf. Commun. (ICC)*, Dublin, Ireland, Jun. 2020.

[8] A. Bourdoux, A. N. Barreto, B. van Liempd, C. de Lima, D. Dardari, D. Belot, E.-S. Lohan, G. Seco-Granados, H. Sarieddeen, H. Wymeersch *et al.*, "6G white paper on localization and sensing," *arXiv preprint arXiv:2006.01779*, 2020.

[9] H. Wymeersch, J. He, B. Denis, A. Clemente, and M. Juntti, "Radio localization and mapping with reconfigurable intelligent surfaces," *IEEE Vehicular Technology Magazine*, 2020.

[10] F. Guidi and D. Dardari, "Radio positioning with EM processing of the spherical wavefront," *arXiv preprint arXiv:1912.13331*, 2019.

[11] Z. Abu-Shaban, K. Keykhosravi, M. F. Keskin, G. C. Alexandropoulos, G. Seco-Granados, and H. Wymeersch, "Near-field localization with a reconfigurable intelligent surface acting as lens," *arXiv preprint arXiv:2010.05617*, 2020.

[12] J. He, H. Wymeersch, L. Kong, O. Silvén, and M. Juntti, "Large intelligent surface for positioning in millimeter wave MIMO systems," in *Proc. IEEE VTC-Spring*, Antwerp, Belgium, May 2020.

[13] W. Wang and W. Zhang, "Joint beam training and positioning for intelligent reflecting surfaces assisted millimeter wave communications," *arXiv preprint arXiv:2009.03536*, 2020.

[14] H. Wymeersch and B. Denis, "Beyond 5G wireless localization with reconfigurable intelligent surfaces," in *IEEE Int. Conf. Commun. (ICC)*, Dublin, Ireland, Jun. 2020.

[15] A. Elzanaty, A. Guerra, F. Guidi, and M.-S. Alouini, "Reconfigurable intelligent surfaces for localization: Position and orientation error bounds," *arXiv preprint arXiv:2009.02818*, 2020.

[16] "RIS Enabled SISO Localization," 2020. [Online]. Available: https://github.com/KamranKeykhosravi/RIS-Enabled-SISO-Localization

[17] A. Fascista, A. Coluccia, H. Wymeersch, and G. Seco-Granados, "Millimeter-wave downlink positioning with a single-antenna receiver," *IEEE Trans. Wireless Commun.*, vol. 18, no. 9, pp. 4479–4490, 2019.

[18] K. B. Petersen and M. S. Pedersen, *The Matrix Cookbook*, November 15 2012. [Online]. Available: http://www.math.uwaterloo.ca/~hwolkowi/matrixcookbook.pdf